

# Detecting the axion field with waveguide apparatus

André H. Gomes\*

Departamento de Física,  
Universidade Federal de Ouro Preto, 35402-163,  
Ouro Preto, Minas Gerais, Brazil

Winder A. Moura-Melo†

Departamento de Física,  
Universidade Federal de Viçosa, 36570-900,  
Viçosa, Minas Gerais, Brazil

We demonstrate that a conventional hollow conductor waveguide filled with a material exhibiting the coexistence of chiral magnetic and anomalous quantum Hall effects supports the propagation of transverse electromagnetic modes within its interior. This simple setup provides an optically feasible and direct method to probe the simultaneous presence of these phenomena, potentially enabling the detection of the axion field in the condensed matter realm.

*Introduction.* Recently, the chiral magnetic effect (CME) and the anomalous quantum Hall effect (AQHE) have been predicted to occur simultaneously in antiferromagnetic (AFM) insulators with spin-orbit coupling (SOC), with fluctuations of their order parameter (Néel field) linked to the dynamical axion field [1] (for a review see Ref. [2]). Indeed, an analogue of the axion field has been previously predicted to occur in topological magnetic insulators. There, magnetic fluctuations couple to the electromagnetic field likewise the axionic field does [3]. In addition, Weyl semimetals (WSMs) with broken time reversal and space reflection symmetries could also host the coexistence of both effects [4–6].

The anomalous Hall effect arises when time-reversal symmetry is broken by SOC effects, typically observed in the ferromagnetic phase of certain materials. Additionally, topologically protected charged edge states lead to quantized Hall conductivity (for a review, see Ref. [7]). In turn, CME emerges as a consequence of chiral anomaly yielding an imbalance of right- and left-handed chiral fermions under a magnetic field. In addition, this imbalance is linked to the topology of gauge fields by the Atiyah-Singer index theorem, ensuring that the resulting chiral current is dissipationless [8, 9]. Evidence of such an effect in the quark-gluon plasma have been reported in Refs. [10, 11]. More recently, its detection has also been associated with dark matter phenomenon [12], where presumably axionic dark particles would induce an alternating current along magnetic fields in stars and galaxies. Although originally rooted in the framework of high energy physics, this effect has also been recently observed in condensed matter: the Weyl semimetal  $\text{ZrTe}_5$  conductivity is proportional to the applied magnetic field squared,  $|\mathbf{B}|^2$ , a clear signature of CME, as reported in Ref. [13]. In addition, the optical properties encompassed by the Fresnel coefficients are modified in the presence of such a chiral magnetic current [14].

In turn, waveguide devices are widely used to control the profile, the intensity, and the spot of electromagnetic waves designed to characterize a given sample, to send and receive information, and so forth. For that, transverse electromagnetic (TEM) modes appear to be the most suitable ones for several applications since they ensure high efficiency and minimize losses and dispersion along the guide. However, pure TEM waves are idealized modes which would propagate only under ideal circumstances of both media (vacuum or another linear, isotropic, and homogeneous medium) and boundary conditions (perfect conductor). In practice, due to the finite conductivity of real conductors the best one can do is using suitable materials and geometries that allow almost perfect TEM waves to flow.

Let us recall that TEM modes are not allowed to propagate in any guide composed of a single conductor, as stemming from limitations of Laplace's equation in bounded geometries without sources [15, 16]. However, this may be bypassed provided that one departs from usual Maxwell's electrodynamics [17, 18]. This can be achieved, for example, by extending Maxwell's theory to include axion-like electrodynamics [19], which has been widely used to describe the topological magnetoelectric effect coming about whenever light interacts with topological insulators, Weyl semimetals, and other peculiar materials [20]. Other recent proposals to achieve TEM modes flow include all-dielectric coaxial cables made from omnidirectional reflecting mirrors [21] and metamaterials with extremely large anisotropies [22].

In this article, we propose a simple and feasible apparatus designed to optically probe the coexistence of CME and AQHE under the action of a light beam. Indeed, we show that a hollow conductor tube filled with a material supporting both effects allows the propagation of TEM modes in its interior, otherwise forbidden in conventional media. The observation of TEM under these conditions constitutes direct evidence of the axion field in the condensed matter realm by purely optical means, avoiding intricate setups like those typically used in electronic transport and related measurements.

\* [andre.gomes@ufop.edu.br](mailto:andre.gomes@ufop.edu.br)

† [winder@ufv.br](mailto:winder@ufv.br)

*Model and conditions for TEM modes.* Let us start off by augmenting Maxwell's electrodynamics with the inclusion of the so-called axion term [2, 3, 19, 20]:

$$S_\theta = \sqrt{\frac{\varepsilon}{\mu}} \frac{\alpha}{\pi} \int dt d^3x \theta(\mathbf{x}, t) \mathbf{E} \cdot \mathbf{B}, \quad (1)$$

where  $\alpha = e^2/4\pi\epsilon\hbar v$  is the material fine structure constant and  $v = 1/\sqrt{\mu\varepsilon}$ . Whenever it comes from a constant background 4-vector  $\mathbf{b}^\mu = (\mathbf{b}_0, \mathbf{b})$  coupled to space-time coordinates, like

$$\theta(\mathbf{x}, t) = 2(\mathbf{b} \cdot \mathbf{x} - \mathbf{b}_0 t), \quad (2)$$

one has a non-dynamical axion field,  $\theta$ . Since  $\mathbf{b}^\mu$  is a constant 4-vector it explicitly breaks Lorentz invariance; however, it respects gauge symmetry so that electric charge is conserved. For simplicity of notation, from now on we define  $b^\mu = (2\alpha/\pi)\mathbf{b}^\mu$ .

By virtue of the axion term, Gauss' law acquires an extra charge density,

$$\frac{\rho_\theta}{\varepsilon} = v\mathbf{b} \cdot \mathbf{B}, \quad (3)$$

while Ampère-Maxwell's law is augmented by an extra current,

$$\mu\mathbf{J}_\theta = \frac{1}{v}(b_0\mathbf{B} - \mathbf{b} \times \mathbf{E}). \quad (4)$$

Even though originally proposed as a model for probing novel phenomena concerning violations of Lorentz symmetry [23–27], presumably originated at the very high-energy regime of the primordial universe, such an electrodynamics has also been used as an effective description of exotic states of matter [2, 3, 20, 28]. More specifically,  $b_0$ -term describes the (static) CME [9] while  $\mathbf{b}$ -terms are associated to AHE [7, 29]. For instance, in certain AFM compounds with strong SOC effects bringing about space-time variations for the order parameter (Néel field),  $\mathbf{n}(\mathbf{x}, t)$ , the local fluctuations of the magnetization are regarded as the realization of the (dynamical) axion field, i.e.,  $\delta\mathbf{n}(\mathbf{x}, t) \propto \delta\theta(\mathbf{x}, t)$  [1, 2], which may be encompassed by Eq. (2) in the linear response regime. In turn, for WSMs  $2\hbar b_0$  represents the shift in energy (also proportional to the chemical potential difference) of two Weyl nodes in a  $P$ -breaking WSM while  $2\mathbf{b}$  is the separation distance in reciprocal space of two Weyl nodes in a  $T$ -breaking WSM [4–6].

Now, we shall establish the conditions which allow TEM modes to propagate through the interior of hollow metallic guides filled with a material supporting AQHE and CME concomitantly, and which are linked to the axion field as prescribed by Eq. (2). Fig. 1 depicts the specific case of a circular cylindrical guide. The incident light beam has frequency  $\omega$  lying within the transparency band gap of the core material, i.e.,  $\omega_p < \omega < \omega_F$ , where  $\omega_p$  and  $\omega_F$  are the plasma and Fermi frequencies of the

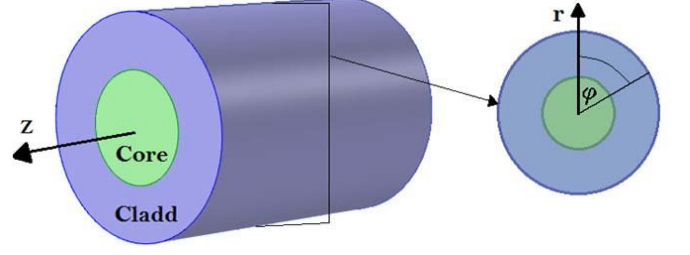


FIG. 1. Schematics of a cylindrical waveguide consisting of a hollow metallic wall (gray cladd) filled with a compound supporting the coexistence of CME and AQHE (the core depicted in light green color). A light beam is imparted to the compound and TEM modes propagate through it when a magnetic field,  $\mathbf{B} = B_0\hat{\mathbf{z}}$ , is turned on.

material (further details below). A general TEM sinusoidal wave propagating along the  $\hat{\mathbf{z}}$ -direction is given by

$$\mathbf{E}(\mathbf{x}, t) = \mathcal{E}(\mathbf{x}_\perp) e^{i(kz - \omega t)} \quad \text{and} \quad \mathcal{E} \cdot \hat{\mathbf{z}} = 0, \quad (5)$$

$$\mathbf{B}(\mathbf{x}, t) = \mathcal{B}(\mathbf{x}_\perp) e^{i(kz - \omega t)} \quad \text{and} \quad \mathcal{B} \cdot \hat{\mathbf{z}} = 0, \quad (6)$$

where  $\mathbf{x}_\perp = (x, y) = (r \cos \varphi, r \sin \varphi)$  in Cartesian and cylindrical coordinates, respectively. The guide is assumed to be a perfect conductor, so that the homogeneous boundary conditions are [30]

$$\hat{\mathbf{n}} \times \mathcal{E}|_{\mathcal{S}} = 0, \quad \hat{\mathbf{n}} \cdot \mathcal{B}|_{\mathcal{S}} = 0, \quad (7)$$

where  $\hat{\mathbf{n}}$  is the unity normal vector at the guide walls  $\mathcal{S}$ .

In turn, inside the guide filled with the suitable material, Faraday's and Ampère-Maxwell's laws, augmented by the current arising from the axionic action, Eq. (4), in the linear response regime, yield [31]

$$ik\mathcal{E} - i\omega\mathcal{B} \times \hat{\mathbf{z}} = 0, \quad (8)$$

$$ik\mathcal{B} + i\frac{\omega}{c^2}\mu_r\epsilon_r^*\mathcal{E} \times \hat{\mathbf{z}} = \frac{1}{v}(b_0\mathcal{B} \times \hat{\mathbf{z}} - b_z\mathcal{E}), \quad (9)$$

with  $\mu_r \equiv \mu/\mu_0$ , and where the complex relative permittivity is defined as  $\epsilon_r^*(\omega) \equiv \epsilon_r(\omega) + i\sigma(\omega)/\varepsilon_0\omega$ , with  $\epsilon_r \equiv \varepsilon/\varepsilon_0$  denoting its real part and  $\sigma$  the material conductivity [32]. Mutual consistency of Eqs. (8) and (9) requires

$$\omega = \frac{ck}{\sqrt{\mu_r\epsilon_r^*(\omega)}} \quad \text{and} \quad b_0 = \frac{\omega}{k}b_z. \quad (10)$$

Since we shall obtain transmitted power by TEM waves throughout the guides, let us focus our analysis on the optically transparent regime of the material, i.e.,  $\omega_p < \omega < \omega_F$ . The plasma frequency,  $\omega_p$ , defines the threshold below which reflection dominates due to collective oscillations of free electrons (plasmons), whereas the Fermi frequency,  $\omega_F = E_F/\hbar$ , represents the energy scale associated with the Fermi energy. Indeed, whenever  $\omega < \omega_F$ , the single-band (Drude-like) term dominates,

and interband transitions are minimal, preserving transparency. Assuming the validity of Drude approximation,  $\epsilon_r^*(\omega) \approx \epsilon_r(1 - \omega_p^2/\omega^2)$  [33, 34], so that  $ck \gg \omega_p$ . Then, the first condition in Eqs. (10) yields a single propagating TEM mode with frequency

$$\omega = \frac{ck}{\sqrt{\mu_r \epsilon_r}} + \mathcal{O}\left(\frac{\omega_p^2}{c^2 k^2}\right) \approx \frac{k}{\sqrt{\mu \epsilon}} = vk, \quad (11)$$

so that light propagates throughout the bulk without frequency cutoff at maximum speed  $v = 1/\sqrt{\mu \epsilon}$ .

Additionally, TEM modes also require that the second condition in Eq. (10) holds identically,  $b_0 = \omega b_z/k = vb_z$ , which can be fulfilled if  $\omega/k = v = \text{constant}$ , given that  $b_0$  and  $\mathbf{b}$  are assumed to be constant parameters. Eventually, Eq. (8) implies that the electric and magnetic fields must be orthogonal to each other and to the propagation direction within the waveguide as it should be for a TEM mode:

$$\mathcal{E} = v\mathbf{B} \times \hat{\mathbf{z}}. \quad (12)$$

Before proceeding further, we should discuss the feasibility of the condition  $b_0 = \omega b_z/k = vb_z$ . Recall that in WSMs,  $2\hbar b_0$  is the energy gap ( $\sim$  chemical potential difference) while  $2b_z$  represents the shift in momentum space (along  $z$ ) between two Weyl nodes. Therefore, to satisfy the condition above, tuning of one or both parameters may be in order. This can be accomplished in practice with applied magnetization/magnetic field, pressure and so forth (see, for instance, Refs. [35, 36]). Indeed, even huge variations in  $b$ -parameters could be achieved by suitable thermal fluctuations, at least in a specific class of WSMs like the compound  $\text{Cd}_2\text{Re}_2\text{O}_7$ , as reported in Ref. [37].

*Results and Discussion.* In the following, we explicitly discuss three waveguide geometries that support TEM modes under the application of a uniform magnetic field,  $\mathbf{B}_{\text{ext}} = B_0 \hat{\mathbf{z}}$ , as long as the guide is filled by a core material with  $b_0 = vb_z$ . In this situation, Maxwell's equations now read:

$$\nabla_{\perp} \cdot \mathcal{E} = \mathbf{b}_{\perp} \cdot (v\mathbf{B}) + b_0 B_0, \quad \nabla_{\perp} \times \mathcal{E} = 0, \quad (13)$$

$$\nabla_{\perp} \times (v\mathbf{B}) = b_0 B_0 \hat{\mathbf{z}} - \mathbf{b}_{\perp} \times \mathcal{E}, \quad \nabla_{\perp} \cdot \mathbf{B} = 0. \quad (14)$$

Physically,  $\mathbf{B}_{\text{ext}} = B_0 \hat{\mathbf{z}}$  couples to the axion field and yields effective source terms, thus circumventing the prohibition of TEM modes inside hollow metallic guides. In single-walled guides, like in cylindrical and rectangular geometries, one also needs to set  $\mathbf{b}_{\perp} \cdot \mathbf{B} = 0$  to ensure TEM modes, whereas in a slab-type guide this condition is not required.

*Cylindrical waveguide.* The homogeneous Maxwell's equations yield the boundary conditions (7), specifically  $\hat{\mathbf{r}} \times \mathcal{E} = 0$  and  $\hat{\mathbf{r}} \cdot \mathbf{B} = 0$  at the walls of a cylinder of radius  $R$ . Taking  $\mathbf{b}_{\perp} \cdot \mathbf{B} = 0$  into account, the non-homogeneous equations become analogous to those describing electrostatic and magnetostatic fields inside a wire with uniform

charge and current densities given by  $\rho/\epsilon = b_0 B_0$  and  $\mu \mathbf{J} = (b_0 B_0/v) \hat{\mathbf{z}}$ . The solutions are readily obtained as  $\mathcal{E} = (\rho r/2\epsilon) \hat{\mathbf{r}}$  and  $\mathbf{B} = (\mu J r/2) \hat{\boldsymbol{\varphi}}$  along the transverse coordinates  $(r, \varphi)$  [16]. Augmenting them with the propagating factor along  $z$ , one obtains the field solutions propagating inside the waveguide as

$$\mathbf{E}(\mathbf{x}, t) = \frac{1}{2} b_0 B_0 r \cos(kz - \omega t) \hat{\mathbf{r}}, \quad (15)$$

$$\mathbf{B}(\mathbf{x}, t) = \frac{1}{2v} b_0 B_0 r \cos(kz - \omega t) \hat{\boldsymbol{\varphi}} + B_0 \hat{\mathbf{z}}. \quad (16)$$

The radiation power density  $\mathcal{P}_{\text{rad}} = \mathbf{S} \cdot \hat{\mathbf{z}} = \frac{1}{\mu} (\mathbf{E} \times \mathbf{B}) \cdot \hat{\mathbf{z}} = \frac{1}{4\mu v} (b_0 B_0)^2 r^2 \cos^2(kz - \omega t)$  yields the time-averaged transmitted power through the entire guide:

$$P = \int \langle \mathcal{P}_{\text{rad}} \rangle_t dA = \frac{\pi R^4}{16\mu v} (b_0 B_0)^2. \quad (17)$$

It is noteworthy that such an intensity is also proportional to  $(B_0)^2$  and comes from topological grounds brought about by the axion anomaly according to action (1), likewise the CME chiral conductivity reported in Ref. [13]. Its optical probing, as predicted above, provides an unambiguous and direct signature of the axion field realization by the material filling the waveguide.

*Rectangular waveguide.* The case of a rectangular waveguide with width  $w$  and height  $h$  can be readily solved using an electrostatic potential  $\Phi(x, y)$  that vanishes at the guide walls. By setting  $\mathcal{E} = -\nabla_{\perp} \Phi$  and  $\mathbf{b}_{\perp} \cdot \mathbf{B} = 0$ , the nonhomogeneous Maxwell's equations reduce to

$$\nabla_{\perp}^2 \Phi(x, y) = -b_0 B_0. \quad (18)$$

Equation (18) is analogous to the Saint-Venant torsion problem in solid mechanics, where  $\Phi$  plays the role of Prandtl's stress function, and the source term is  $-2Gk$  with  $G$  the shear modulus and  $k$  the (constant) twist rate [38]. The solution is well-known in the literature [39] and it is

$$\Phi(x, y) = \sum_{n=1,3,\dots} \frac{8b_0 B_0 w^2}{(n\pi)^3} \sin \frac{n\pi x}{w} \left[ \cosh \frac{n\pi y}{w} - 1 + \left( \frac{1 - \cosh \frac{n\pi h}{w}}{\sinh \frac{n\pi h}{w}} \right) \sinh \frac{n\pi y}{w} \right]. \quad (19)$$

The corresponding expressions for  $\mathbf{E}$  and  $\mathbf{B} = \hat{\mathbf{z}} \times \mathbf{E}/v$  are not very revealing. Figure 2 depicts their spatial behavior in a cross-section of the guide (considering the first 20 terms of the summation above). The field lines reveal an effective line-like charge and current densities located along the guide axis (center of the images) due to the coupling between the applied magnetic field and the axion field. Of course, the transmitted power through the guide scales with  $(B_0)^2$ , as in the previous geometry.

*Slab waveguide.* For a slab waveguide, the condition  $\mathbf{b}_{\perp} \cdot \mathbf{B} = 0$  is no longer necessary. The slab we consider

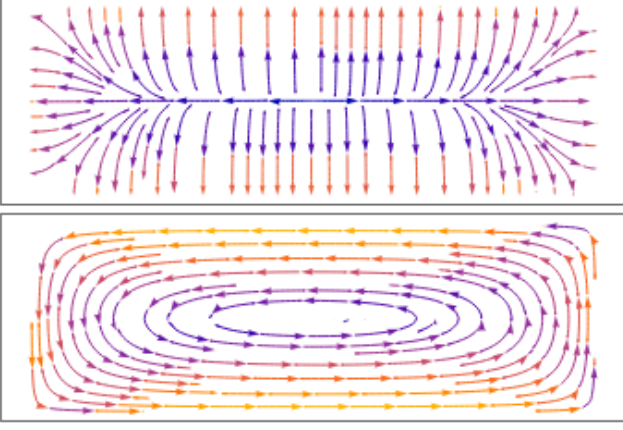


FIG. 2. Cross-sectional profiles of the electric (top) and magnetic (bottom) fields of a propagating TEM wave inside a rectangular waveguide with a width-to-height ratio of 3:1.

has height  $h$ , and it is open along the  $x$ - and  $z$ -directions. Since the fields are independent of  $x$ , Gauss' and Faraday's laws (13) simplify to

$$\partial_y \mathcal{E}_y = b_y \mathcal{E}_x - b_x \mathcal{E}_y + b_0 B_0, \quad \partial_y \mathcal{E}_x = 0, \quad (20)$$

once  $\mathcal{E} = v\mathbf{B} \times \hat{\mathbf{z}}$  is used. Since Faraday's law imposes the boundary condition  $\mathcal{E}_x|_{y=\{0,h\}} = 0$ , it follows that  $\mathcal{E}_x = 0$  throughout the slab, so the  $b_y$  component plays no role at all. Writing  $\mathcal{E}_y(y) = -d\Phi(y)/dy$ , Gauss's law then reads:

$$\frac{d^2\Phi}{dy^2} + b_x \frac{d\Phi}{dy} = -b_0 B_0. \quad (21)$$

Setting slab top and bottom walls at the same potential, say,  $\Phi(0) = \Phi(h) = 0$ , one obtains [40]

$$\Phi(y) = \left( \frac{1 - e^{-b_x y}}{1 - e^{-b_x h}} h - y \right) \frac{b_0 B_0}{b_x}, \quad (22)$$

yielding the electric and magnetic fields propagating inside the slab to be

$$\mathbf{E}(y, z, t) = - \left( \frac{b_x h e^{-b_x y}}{1 - e^{-b_x h}} - 1 \right) \frac{b_0 B_0}{b_x} \cos(kz - \omega t) \hat{\mathbf{y}}, \quad (23)$$

$$\mathbf{B}(y, z, t) = \left( \frac{b_x h e^{-b_x y}}{1 - e^{-b_x h}} - 1 \right) \frac{b_0 B_0}{v b_x} \cos(kz - \omega t) \hat{\mathbf{x}}. \quad (24)$$

Thus, inside this slab waveguide TEM mode flows with  $\mathcal{P}_{\text{rad}} = \frac{1}{\mu v} [b_x h e^{-b_x y} / (1 - e^{-b_x h}) - 1]^2 (b_0 B_0 / b_x)^2 \cos^2(kz - \omega t)$ , so that the time-averaged transmitted power per unit length along  $x$  reads:

$$\frac{dP}{dx} = \frac{h}{2\mu v} \left[ \frac{b_x h}{2} \coth\left(\frac{b_x h}{2}\right) - 1 \right] \left( \frac{b_0 B_0}{b_x} \right)^2. \quad (25)$$

Besides  $b_0$  (and  $b_z$ , satisfying  $b_0 = v b_z$ ), the slab geometry also offers a way to probe the transverse  $\mathbf{b}_\perp$  parameters, namely, that perpendicular to its walls. In addition, notice that  $dP/dx$  is analytic at  $b_x = 0$  (even though the fields are not) and, in this limit, reduces to  $dP/dx = (b_0 B_0)^2 h^3 / 24\mu v$  [41].

*Concluding remarks.* Whenever a usual metallic waveguide is filled with a material encompassing both chiral magnetic and anomalous quantum Hall effects, then TEM modes are shown to propagate throughout its bulk. We illustrate our findings by considering the cases of cylindrical, rectangular, and slab-type geometries. In every case, the guide is immersed in a homogeneous axial magnetic field that couples to the axion-like field. The transmitted power by TEM waves is proportional to  $(B_0)^2$ , which is a direct and unambiguous signature of both CME and AQHE coexisting in the material.

Experimental observation of these predictions appears to be direct evidence of the axion field in the condensed matter realm by purely optical means, avoiding intricate setups like those typically used in electronic transport and related measurements. In addition, once AQHE can also arise from a nonzero integral of Berry curvature, it should be stressed that usual transport measurements alone cannot decisively relate it to an axion field [42]. Thus, other experimental evidence is mandatory to unambiguously trace both effects back to the axial anomaly.

*Acknowledgments.* The authors thank the Brazilian agencies CAPES, CNPq, FAPEMIG, INCT/CNPq – *Spintrônica e Nanoestruturas Magnéticas Avançadas (INCT-SpinNanoMag)*, and Rede Mineira de Nanomagnetismo/FAPEMIG for financial support.

- 
- [1] A. Sekine and K. Nomura, Chiral Magnetic Effect and Anomalous Hall Effect in Antiferromagnetic Insulators with Spin-Orbit Coupling, *Phys. Rev. Lett.* **116**, 096401 (2016).  
 [2] A. Sekine and K. Nomura, Axion electrodynamics in

- topological materials, *Journal of Applied Physics* **129**, 141101 (2021).  
 [3] R. Li, J. Wang, X.-L. Qi, and S.-C. Zhang, Dynamical axion field in topological magnetic insulators, *Nature Phys* **6**, 284 (2010).



- [4] A. A. Zyuzin, S. Wu, and A. A. Burkov, Weyl semimetal with broken time reversal and inversion symmetries, *Phys. Rev. B* **85**, 165110 (2012).
- [5] G. Chang, B. Singh, S.-Y. Xu, G. Bian, S.-M. Huang, C.-H. Hsu, I. Belopolski, N. Alidoust, D. S. Sanchez, H. Zheng, H. Lu, X. Zhang, Y. Bian, T.-R. Chang, H.-T. Jeng, A. Bansil, H. Hsu, S. Jia, T. Neupert, H. Lin, and M. Z. Hasan, Magnetic and noncentrosymmetric Weyl fermion semimetals in the *RAiGe* family of compounds (*R* = rare earth), *Phys. Rev. B* **97**, 041104 (2018).
- [6] S. Heidari and R. Asgari, Nonlinear chiral photocurrent in parity-violating magnetic Weyl semimetals, *Phys. Rev. B* **106**, 195148 (2022).
- [7] N. Nagaosa, J. Sinova, S. Onoda, A. H. MacDonald, and N. P. Ong, Anomalous Hall effect, *Rev. Mod. Phys.* **82**, 1539 (2010).
- [8] K. Fukushima, D. E. Kharzeev, and H. J. Warringa, Chiral magnetic effect, *Phys. Rev. D* **78**, 074033 (2008).
- [9] D. E. Kharzeev, The Chiral Magnetic Effect and anomaly-induced transport, *Progress in Particle and Nuclear Physics* **75**, 133 (2014).
- [10] R. Belmont, Charge-dependent anisotropic flow studies and the search for the Chiral Magnetic Wave in ALICE, *Nuclear Physics A* **931**, 981 (2014).
- [11] L. Adamczyk *et al.* (STAR Collaboration), Observation of Charge Asymmetry Dependence of Pion Elliptic Flow and the Possible Chiral Magnetic Wave in Heavy-Ion Collisions, *Phys. Rev. Lett.* **114**, 252302 (2015).
- [12] D. K. Hong, S. H. Im, K. S. Jeong, and D.-h. Yeom, Detecting axion dark matter with chiral magnetic effects, *Phys. Rev. D* **110**, 055036 (2024).
- [13] Q. Li, D. E. Kharzeev, C. Zhang, Y. Huang, I. Pletikosić, A. V. Fedorov, R. D. Zhong, J. A. Schneeloch, G. D. Gu, and T. Valla, Chiral magnetic effect in  $\text{ZrTe}_5$ , *Nature Phys* **12**, 550 (2010).
- [14] P. D. S. Silva, R. A. Pereira, and M. M. Ferreira, Optical reflection signature of an axion dielectric with magnetic current, *Phys. Rev. B* **110**, 174427 (2024).
- [15] J. D. Jackson, *Classical Electrodynamics* (John Wiley & Sons, 1999).
- [16] D. J. Griffiths, *Introduction to Electrodynamics* (Pearson Education, 2013).
- [17] A. Martín-Ruiz, M. Cambiaso, and L. F. Urrutia, Electro- and magnetostatics of topological insulators as modeled by planar, spherical, and cylindrical  $\theta$  boundaries: Green's function approach, *Phys. Rev. D* **93**, 045022 (2016).
- [18] S. Filipini and M. Cambiaso, Polarization rotation and exact transverse electromagnetic wave solutions in topological insulators, *Phys. Rev. B* **109**, 235108 (2024).
- [19] F. Wilczek, Two applications of axion electrodynamics, *Phys. Rev. Lett.* **58**, 1799 (1987).
- [20] N. P. Armitage, E. J. Mele, and A. Vishwanath, Weyl and Dirac semimetals in three-dimensional solids, *Rev. Mod. Phys.* **90**, 015001 (2018).
- [21] M. Ibanescu, Y. Fink, S. Fan, E. L. Thomas, and J. D. Joannopoulos, An All-Dielectric Coaxial Waveguide, *Science* **289**, 415 (2000).
- [22] P. B. Catrysse and S. Fan, Transverse Electromagnetic Modes in Aperture Waveguides Containing a Metamaterial with Extreme Anisotropy, *Phys. Rev. Lett.* **106**, 223902 (2011).
- [23] R. Jackiw, Chern-Simons violation of Lorentz and PCT symmetries in electrodynamics, *Comments Mod. Phys.* **A 1**, 1 (1999), [arXiv:hep-ph/9811322](https://arxiv.org/abs/hep-ph/9811322).
- [24] S. M. Carroll, G. B. Field, and R. Jackiw, Limits on a Lorentz- and parity-violating modification of electrodynamics, *Phys. Rev. D* **41**, 1231 (1990).
- [25] M. M. Ferreira, J. A. Helayël-Neto, C. M. Reyes, M. Schreck, and P. D. Silva, Unitarity in Stückelberg electrodynamics modified by a Carroll-Field-Jackiw term, *Physics Letters B* **804**, 135379 (2020).
- [26] Soares, David M., Borges, L. H. C., Dallabona, G., and Brito, L. C. T., Material boundaries in Carroll-Field-Jackiw Lorentz-violating electrodynamics, *Eur. Phys. J. Plus* **139**, 152 (2024).
- [27] A. Kostelevy, R. Lehnert, M. Schreck, and B. Seradjeh, *Physical interpretation of large Lorentz violation via Weyl semimetals* (2024), [arXiv:2412.18034 \[hep-ph\]](https://arxiv.org/abs/2412.18034).
- [28] P. D. S. Silva, M. M. Ferreira, M. Schreck, and L. F. Urrutia, Magnetic-conductivity effects on electromagnetic propagation in dispersive matter, *Phys. Rev. D* **102**, 076001 (2020).
- [29] Z. Qiu, G. Cao, and X.-G. Huang, Electrodynamics of chiral matter, *Phys. Rev. D* **95**, 036002 (2017).
- [30] Indeed, finite conductivity does not jeopardize our results concerning TEM modes since it only imparts usual sources and dissipation, as discussed in textbooks [15, 16].
- [31] Strictly speaking, Eq. (9) provides an accurate approximation when spatial variations in the material's magnetization  $\mathbf{M}$  are negligible ( $\nabla \times \mathbf{M} \approx 0$ ), and the response to electric fields is linear. Under these conditions, the combined free, polarization, and magnetization currents result in  $\mathbf{J} = [\sigma - i\omega\epsilon_0(\epsilon_r - 1)]\mathbf{E}$ . Substituting this into Ampère-Maxwell's equation leads to Eq. (9), given the definition of  $\epsilon_r^*(\omega)$ .
- [32] N. Ashcroft and N. Mermin, *Solid State Physics* (Cengage Learning, 2011).
- [33] O. V. Kotov and Y. E. Lozovik, Dielectric response and novel electromagnetic modes in three-dimensional Dirac semimetal films, *Phys. Rev. B* **93**, 235417 (2016).
- [34] O. V. Kotov and Y. E. Lozovik, Giant tunable nonreciprocity of light in Weyl semimetals, *Phys. Rev. B* **98**, 195446 (2018).
- [35] M. P. Ghimire, J. I. Facio, J.-S. You, L. Ye, J. G. Checkelsky, S. Fang, E. Kaxiras, M. Richter, and J. van den Brink, Creating Weyl nodes and controlling their energy by magnetization rotation, *Phys. Rev. Res.* **1**, 032044 (2019).
- [36] E. Cheng, L. Yan, X. Shi, R. Lou, A. Fedorov, M. Behnami, J. Yuan, P. Yang, B. Wang, J.-G. Cheng, Y. Xu, Y. Xu, W. Xia, N. Pavlovskii, D. C. Peets, W. Zhao, Y. Wan, U. Burkhardt, Y. Guo, S. Li, C. Felser, W. Yang, and B. Büchner, Tunable positions of Weyl nodes via magnetism and pressure in the ferromagnetic Weyl semimetal  $\text{CeAlSi}$ , *Nature Comm.* **15**, 1467 (2024).
- [37] S. Chen, A. Bouhon, R.-J. Slager, and B. Monserat, Non-Abelian braiding of Weyl nodes via symmetry-constrained phase transitions, *Phys. Rev. B* **105**, L081117 (2022).
- [38] S. Timoshenko and J. N. Goodier, *Theory of Elasticity* (McGraw-Hill, 1951).
- [39] C. C. Ike, Solving Saint Venant torsion problems for rectangular beams using single finite Fourier sine transform method, *Journal of Mechatronics and Artificial Intelligence in Engineering* **5**, 31–41 (2024).
- [40] Recall that even an ordinary slab waveguide with walls

at different potentials supports TEM mode propagation. This is not the case, however, when the walls are at the same potential.

- [41] It can be checked that this result agrees with that for a rectangular guide of width  $w \rightarrow \infty$  in the  $\mathbf{b}_\perp \cdot \mathbf{B} = 0$  case. TEM solutions are obtained by solving  $d^2\Phi/dy^2 = -b_0B_0$  subject to  $\Phi(0) = \Phi(h) = 0$ , yielding  $\Phi(y) = -b_0B_0y(y-h)/2$ . The fields are then  $\mathbf{E} =$

$b_0B_0(y-h/2)\cos(kz-\omega t)\hat{\mathbf{y}}$  and  $\mathbf{B} = (\hat{\mathbf{z}} \times \mathbf{E})/v$ , and the time-averaged transmitted power per width-length is  $dP/dx = (b_0B_0)^2h^3/24\mu v$ .

- [42] K. Deng, J. S. Van Dyke, D. Minic, J. J. Heremans, and E. Barnes, Exploring self-consistency of the equations of axion electrodynamics in Weyl semimetals, [Phys. Rev. B \*\*104\*\*, 075202 \(2021\)](#).